High-resolution photoelectron spectroscopy of NO_3^- vibrationally excited along its ν_3 mode

Jascha A. Lau,[1,†] Martin DeWitt,[1] Peter R. Franke,[2] John F. Stanton,[2] and Daniel M. Neumark[1,3,*]

[1] Department of Chemistry, University of California, Berkeley, CA 94720, USA

[2] Department of Chemistry, University of Florida, Gainesville, FL 32611, USA

[3] Chemical Sciences Division, Lawrence Berkeley National Laboratory, Berkeley, CA 94720, USA

[†] Present address: Fritz-Haber-Institut der Max-Planck-Gesellschaft, Faradayweg 4-6, 14195 Berlin, Germany

[*]Corresponding author: dneumark@berkeley.edu

Abstract

The nitrate (NO_3) radical has long been the subject of both experimental and theoretical studies due to its complex electronic structure resulting from vibronic interactions between the $\tilde{X}\ ^2A_2'$ and $\tilde{B}\ ^2E'$ states. In particular, the definite assignment of the fundamental of its degenerate stretching vibration (ν_3) is still under debate. Here, we extend the available spectroscopic information by reporting high-resolution photoelectron spectra of vibrationally pre-excited NO_3^- using the recently developed IR-cryo-SEVI technique. The anions are excited through infrared (IR) excitation near 1350 cm^{-1}, accessing the ν_3 and $2\nu_3(e')$ vibrational levels with band centers at 1350.5 cm^{-1} and ~2700 cm^{-1}, respectively. The IR-cryo-SEVI spectrum for $2\nu_3$ pre-excitation shows clear evidence for an intense 3_2^1 transition. From the position of this feature (30031 cm^{-1}), the electron affinity of NO_3 also determined in this work (31680 cm^{-1}), and the IR excitation energy, we obtain a fundamental frequency of 1051 cm^{-1} for the ν_3 fundamental of the NO_3 radical. This assignment and other features in the IR-cryo-SEVI spectra are supported by spectral simulations based on a vibronic Köppel-Domcke-Cederbaum Hamiltonian. The simulations also show that nearly all features in the IR-cryo-SEVI spectra arise because of pseudo-Jahn-Teller coupling between the $\tilde{X}$ and $\tilde{B}$ state of NO_3. The results and analysis presented here settle a long-standing controversy regarding the ν_3 frequency of NO_3.

1. Introduction

The nitrate (NO_3) radical is of fundamental interest as an atmospherically important species that exhibits unusually complex spectroscopy. Atmospheric NO_3 is photolyzed in daytime, but at nighttime its concentration builds up and it serves as a primary tropospheric oxidizer, reacting to form HNO_3, N_2O_5, and organic nitrates.[1] It was one of the first atmospheric radicals investigated by spectroscopic methods, as some of its absorption lines were already seen as a byproduct in the investigation of ozone in 1882.[2] Since then, NO_3 has been investigated by practically every spectroscopic technique in the physical chemistry toolbox, including infrared (IR) spectroscopy,[3-12] laser-induced and dispersed fluorescence,[13-19] cavity-ringdown spectroscopy,[20-22] matrix isolation spectroscopy,[23, 24] and photoelectron spectroscopy of the NO_3^- anion.[25, 26] Nonetheless, several aspects of NO_3 spectroscopy remain under discussion, most notably the frequency of its ν_3 degenerate stretching vibration. To address this issue, we investigate NO_3 in this work by applying a newly developed spectroscopic method in which the high-resolution photoelectron spectrum of NO_3^-, obtained via slow-electron velocity-map imaging of cryogenically cooled anions (cryo-SEVI),[27] is measured following IR excitation of the ν_3 mode of the NO_3^- anion.

The spectroscopic complexity of NO_3 is exemplified by uncertainties in such basic properties as its equilibrium geometry. For many years, experimental and theoretical studies alternated between a D_{3h}[4, 5, 28-30] and C_{2v}[15, 16, 31-33] equilibrium structure. It was recognized early on that the difficulty in assigning a clear structure comes from the very flat potential energy landscape along the degenerate ν_4 bending and ν_3 stretching modes that connect these two structures.[34] The reason for this flat landscape is the presence of strong vibronic coupling in NO_3. The distortion of the adiabatic $\tilde{X}\ ^2A_2'$ ground-state potential energy surface (PES) arises from a pseudo-Jahn-Teller (pJT) interaction with the $\tilde{B}\ ^2E'$ excited state, which itself is strongly influenced by Jahn-Teller coupling.[34, 35] The question of whether the equilibrium geometry is C_{2v} or D_{3h} has not been settled. However, the issue is purely an academic one; the molecule behaves as a D_{3h} symmetric top.[35]

In 2007, Stanton suggested that the same vibronic interactions also have a profound influence on the ν_3 mode.[35] He predicted the fundamental frequency closer to 1050 cm^{-1}, in notable disagreement with the accepted position of 1492 cm^{-1} at that time and leading to a still ongoing controversy[36, 37] about the correct ν_3 frequency of NO_3. To be more precise, the original assignment assigns the ν_3 fundamental frequency to 1492 cm^{-1} ("Assignment A"), which corresponds to the

strongest IR transition of the molecule[3, 10] and was first observed in laser-induced fluorescence (LIF) spectra.[13, 15] Stanton, on the other hand, proposed that the ν_3 fundamental frequency lies close to 1050 cm^{-1} ("Assignment B") and has vanishing infrared intensity as a result of canceling contributions to the transition dipole moment from the vibronically coupled $\tilde{X}\ ^2A_2'$ and $\tilde{B}\ ^2E'$ states.[35, 38] Consequently, he assigned the strongly IR-active mode at 1492 cm^{-1} to $\nu_3 + \nu_4$, for which such a cancellation does not occur.[38] Another complication adding to this debate is that the frequency of the totally symmetric stretching vibration (ν_1), which appears in the LIF spectra, also lies close to 1050 cm^{-1}.[18]

Ab initio calculations generally seem to support "Assignment B". However, even for computational methods that agree with this assignment, an overall satisfactory description of the NO_3 radical is not always possible. For example, calculations using coupled diabatic potential energy surfaces place the ν_3 fundamental frequency between 1020 and 1040 cm^{-1}, in good agreement with "Assignment B".[39, 40] These calculations also agree with experimental anion photoelectron spectra[41, 42] but predict a large IR intensity for the ν_3 fundamental. Adiabatic calculations of the NO_3 ground state give vibrational frequencies for the ν_3 fundamental close to 1050 cm^{-1} and predict vanishing intensity for ν_3 while the combination band $\nu_3 + \nu_4$ carries significant intensity.[38, 43] However, these adiabatic frequency and intensity calculations suffer from the strong distortion of the ground-state surface caused by vibronic coupling, leading to significant higher-order contributions to the anharmonic ground state potential and dipole moment surface that need to be included for an accurate description.

The ν_3 assignment has also been the focus of several recent experimental studies. As mentioned earlier, LIF spectroscopy was among the first techniques to study the vibrational structure of NO_3.[13, 15, 16] Only recently, higher-resolution LIF emission spectra for $^{14}NO_3$ and $^{15}NO_3$ were published that showed two clearly resolved doublets around 1050 and 1500 cm^{-1}, adding to the ambiguity of the exact location of the ν_3 frequency.[18, 19] In the $^{14}NO_3$ spectra originating from the $\tilde{B}\ ^2E'$ vibrational ground state, vibrational levels at 1051 and 1055 cm^{-1} were assigned to ν_1 and $3\nu_4(a_1')$, and vibrational levels at 1492 and 1500 cm^{-1} were assigned to ν_3 and $2\nu_2$, in accordance with "Assignment A".[18]

Kawaguchi and co-workers were the first to adopt "Assignment B" in the analysis of their IR spectra in 2011. More recently in 2021, Kawaguchi *et al.* reported extremely weak rovibrational

transitions, consistent with a band center of 1054.1 cm^{-1} and about 2000 times smaller than the ones observed for the strongly IR-active vibration at 1492.[11] They assigned the former to ν_3 and the latter to $\nu_3 + \nu_4$, consistent with "Assignment B". However, it should be noted that the observed transitions assigned to ν_3 barely lie above the noise level. In addition, Kawaguchi and co-workers recently published another work in which nearly all vibrational levels up to ~2500 cm^{-1} are assigned based on the new estimate of the ν_3 frequency and all currently available high-resolution IR and LIF spectroscopic data.[12]

Anion photoelectron spectroscopy[25] of NO_3^- and cryo-SEVI, its high-resolution variant,[26] provide a complementary perspective on the spectroscopy of NO_3. These spectra showed well-resolved features from transitions to the ground and excited vibrational levels of the NO_3 ground state. In particular, the vibrational origin (the 0_0^0 transition) and two peaks lying 356 and 1044 cm^{-1} above the origin were observed with cryo-SEVI.[26] The peak at 356 cm^{-1} was assigned to the 4_0^1 transition, a Franck-Condon (FC) forbidden transition that is allowed via pJT coupling to the $v = 0$ level of the $\tilde{B}$ state. Differing anisotropy parameters characterizing the photoelectron angular distributions (PADs) for the 0_0^0 and 4_0^1 transitions are consistent with this interpretation. The PAD for the feature at 1044 cm^{-1} is similar to that of the 4_0^1 transition, and this peak was thus assigned as predominantly arising from the 3_0^1 transition, which is allowed by the same pJT mechanism. This assignment, which is consistent with "Assignment B" of the ν_3 frequency of the neutral, is supported by simulations based on a vibronic Köppel-Domcke-Cederbaum (KDC) Hamiltonian[44] also presented in Ref. 25. However, a small contribution to this peak from the very close-lying FC-allowed 1_0^1 transition was also predicted. Unfortunately, the resolution of the cryo-SEVI experiment was not sufficient to separate these two potential contributions, a result that motivated the current study.

A key result from these photoelectron spectroscopy experiments is that the photodetachment cross section to the $\tilde{X}$ state is considerably lower than that to form the $\tilde{A}\ ^2E'$ and $\tilde{B}\ ^2E'$ states. As a result, transitions allowed by pJT coupling can be more intense than FC-allowed transitions, since the neutral states are mixed with the $\tilde{B}$ vibronic states of NO_3. This trend is amplified in cryo-SEVI experiments, which are typically performed at low eKE. Symmetry dictates that for NO_3 the FC- and pJT-allowed transitions undergo p- and s-wave detachment at low eKE, respectively, and according to the Wigner threshold law,[45] the cross section for p-wave detachment falls more rapidly near the photodetachment threshold. Indeed, one observes that at photodetachment energies close

to the electron affinity, the 4_0^1 and 3_0^1 transitions are considerably more intense than the FC-allowed 0_0^0 transition, consistent with their assignments as pJT-allowed transitions.[26]

We have recently implemented IR-cryo-SEVI, a high-resolution photoelectron spectroscopy technique building on cryo-SEVI in which cryogenically cooled anions are vibrationally pre-excited before photodetachment, and have applied it to OH^- and H_2CCHO^-.[46, 47] Pre-excitation of the ν_3 mode in the NO_3^- anion offers a new route to access vibronic states involving the ν_3 mode in the NO_3 radical with photoelectron spectroscopy and thus provide further insight into its assignment. In contrast to NO_3, the ν_3 vibration of the well-behaved closed-shell NO_3^- anion is strongly IR-active and its frequency has been reported in the literature, with a value of 1349 cm^{-1} for $NO_3^- \cdot Ar$ in the gas phase[48] and 1356 cm^{-1} for NO_3^- in a Ne matrix.[49]

In this work, we report high-resolution photoelectron spectra of vibrationally pre-excited NO_3^- anions. Within a small IR excitation region around 1350 cm^{-1}, we selectively acquire photoelectron spectra for pre-excitation of the ν_3 fundamental or combined pre-excitation of the ν_3 fundamental and $2\nu_3(e')$ overtone. A series of new features is observed in each case corresponding to hot and sequence band transitions. Spectral simulations based on a vibronic Köppel-Domcke-Cederbaum Hamiltonian are in good agreement with the experiment and show that intensity contributions due to pseudo-Jahn-Teller coupling dominate the observed spectra. Most importantly, the experimental and simulated spectra for $2\nu_3(e')$ excitation show a peak that can only be assigned to a 3_2^1 transition, from which the ν_3 fundamental frequency of 1051±4 cm^{-1} is unambiguously deduced for the NO_3 radical.

2. Experimental Methods

The experimental setup for measuring high-resolution spectra of vibrationally excited anions (IR-cryo-SEVI) has been presented previously[46, 47] and is described here only briefly.

Nitrate anions are generated in a supersonic expansion using an Even-Lavie valve coupled with a ring filament ionizer using a 1% mixture of NO_2 in N_2 gas. These anions pass through a skimmer, a radiofrequency (RF) hexapole guide, and a quadrupole mass filter before entering a cryogenically cooled RF octupole ion trap via a gated entrance aperture. The ion trap is held at 5 K and filled with a gas pulse of 20% H_2 in He for buffer gas cooling about 3 ms before the ions enter. After a storage time of ~40 ms, the anions are extracted from the ion trap and then separated by an

orthogonal Wiley-McLaren time-of-flight mass spectrometer. After a ~2 m flight path, the pulsed ion packet is intersected at right angles by the IR excitation laser pulse and photodetachment laser pulses to vibrationally excite and photodetach ions of the desired mass (m/z=62). The laser interaction region is located within a 7-plate velocity-map imaging (VMI) lens that maps the detached photoelectrons onto a position-sensitive detector comprising a gated 2-plate micro-channel plate (MCP) detector and a phosphor screen that is imaged by a CCD camera.[50] To obtain the 2D projections of the photoelectron distributions, every electron detection event on the position-sensitive VMI detector is centroided using the recently introduced hybrid gradient-CoM (HGCM) algorithm.[51] To reduce noise from stray photoelectrons generated by the UV photodetachment laser, the detection chamber was held at a base pressure of 3×10^{-9} Torr. The overall repetition rate of the experiment is 20 Hz, but the infrared excitation laser is run at 10 Hz to enable simultaneous collection of velocity-map images with IR excitation (IR on) and without IR excitation (IR off).

An IR OPO/OPA laser system (LaserVision, 2.8 cm^{-1} bandwidth[46]) pumped by a pulsed Nd:YAG laser (Continuum SureLite SLIII-EX, 10 Hz) is used for vibrational pre-excitation. IR light at ~1350 cm^{-1} is generated by difference frequency mixing of the signal and idler output of the OPA in a $AgGaSe_2$ crystal with typical pulse energies of 500 µJ. For photodetachment in the UV spectral range (285-335 nm), the frequency-doubled output of a tunable dye laser (Radiant Dyes NarrowScan) pumped by the second harmonic of a pulsed Nd:YAG laser (Spectra-Physics Quanta-Ray PRO-290, 20 Hz) is used. Residual fundamental dye laser light is separated from the desired frequency-doubled UV light via a harmonic separator. The UV light is focused with a fused silica lens (f=500 mm) and transmitted into the chamber through a CaF_2 brewster window. The IR and UV beams are counterpropagating and are temporally and spatially overlapped in the laser interaction region.

From the 2D projections of the electron distribution, three-dimensional photoelectron distributions are recovered using the maximum entropy Legendre expanded image reconstruction (MELEXIR) algorithm.[52] The radial part of the reconstructed distribution is related to electron kinetic energy (eKE) by a calibration of eKE against radius for several lines in the O^- photodetachment spectrum at various photodetachment energies.[53] The accuracy of this calibration is estimated to be slightly better than 3 cm^{-1}. The spectra as a function of eKE can then be converted to eBE via $eBE = h\nu - eKE$, where $h\nu$ is the photon energy of the tunable photodetachment laser. To record a cryo-SEVI or IR-cryo-SEVI spectrum, multiple high-resolution spectra where the transitions of interest appear

at low eKE are recorded at various photodetachment energies, taking advantage of the improved eKE resolution of the VMI setup for slower photoelectrons.

The photoelectron angular distribution reports on the anisotropy parameter, β, according to Eq. (1) for the differential cross section:

$$\frac{d\sigma}{d\Omega} = \frac{\sigma_{\text{total}}}{4\pi}\left(1 + \beta P_2(\cos\theta)\right). \quad (1)$$

Here, σ_{total} is the total photodetachment cross section, $P_2(\cos\theta)$ is the second-order Legendre polynomial and θ is defined by the angle between the vectors describing the laser polarization axis and the outgoing electron velocity. The anisotropy parameters can also be extracted from the MELEXIR output for each peak and lie between -1 and 2.

The (IR on) – (IR off) spectra show the effect of IR excitation on the anion photoelectron spectrum. In addition, IR action spectra of the anions can also be obtained by monitoring the integrals of peaks in the IR on spectrum relative to a reference peak as a function of IR wavelength in two ways. In the first case, the depletion of a peak in the IR on vs. IR off spectrum is monitored as a function of IR wavelength. For the second case, any new peak in the IR on spectrum that results from excitation of the anion vibration of interest can be chosen and its integrated signal relative to that of the reference peak in the IR off spectrum can be monitored as a function of IR wavelength. Experimentally, the mid-IR wavelength is determined by measuring the wavelength of the near-IR wavelength coupled out of the OPO cavity with a wavemeter (HighFinesse WS5). For each IR wavelength, complete photoelectron spectra are recorded and processed with around 25 min acquisition time per wavelength. Since the full photoelectron spectrum is stored, derivation of the IR action spectrum based on other peaks is possible in post-processing.

3. Computational Details

Simulations of the spectrum are based on the same vibronic Köppel-Domcke-Cederbaum (KDC) Hamiltonian[44] used in Refs. [54] and [55], which is fully documented in those two publications. The simulations were performed with the xsim module of the CFOUR program system,[56] which was also used to carry out all quantum-chemical calculations.

The only additional modification needed for the present work arises from the nature of the IR-cryo-SEVI experiments. While the simulation of photodetachment from the ground vibrational state of the anion is straightforward (the vibrational basis functions used to solve for the vibronic levels of the neutral are those of the anion)[26] and somewhat more involved in the simulation of the dispersed fluorescence spectrum,[55] the simulation of photodetachment from excited vibrational states of the anion represents a new challenge. When the initial anion state is non-degenerate, one can simply invoke the harmonic approximation, and provide a Lanczos[57] seed vector corresponding to the vibrational state in question. However – and such examples are the ν_3 and $2\nu_3(e')$ states in this paper – the photodetachment of degenerate e' vibrational states is less straightforward. Also here, a Lanczos seed vector representing either one of the ν_{3a} and ν_{3b} or one of the $2\nu_{3a}$ and $2\nu_{3b}$ states can be used. The resulting spectrum is independent of which component of the degenerate anion state is chosen. However, in such cases, the mutually exclusive nature of FC- and vibronically-allowed transitions that exists for non-degenerate states, independent of the final neutral state, is lost. While transitions from e' vibrational anion levels that land on non-degenerate levels of the neutral fall cleanly into one of these two categories, those that land on e' states of the neutral can have contributions from both sources. This requires careful consideration of the transition intensities, as the FC and vibronic contributions can either constructively or destructively interfere.

In the present work, we simply consider the FC and vibronic contributions, associated with transition moments into the $\tilde{X}\ ^2A_2'$ and $\tilde{B}\ ^2E'$ states, respectively, as two separate contributions, which is a useful assumption for the present work as will be seen in Section 4. To simulate a $\tilde{B}$ state spectrum, reflecting only vibronic contributions, only the photodetachment transition moment into the $\tilde{B}$ state contributes while the transition moment into the $\tilde{X}$ state is set to 0. To simulate an $\tilde{X}$ state spectrum, reflecting the FC contributions, the transition moment into the $\tilde{B}$ state is set to 0. The overall photodetachment cross section ratio (equivalent to the ratio of the squared transition moments) is assumed to be $\sigma_{\tilde{X}}/\sigma_{\tilde{X}} = 1/100$ to allow for a direct comparison between the $\tilde{X}$ and $\tilde{B}$ state contributions.

In addition, accurate frequency calculations of the NO_3^- anion are performed using a combination of vibrational perturbation theory (VPT2) and vibrational configuration interaction (VCI), based on a composite-hybrid full quartic force field (QFF), as described in detail in the SI.

4. Results

4.1. High-resolution photoelectron and IR action spectra for ν_3 and $2\nu_3$ pre-excitation

The gas phase IR spectrum of NO_3^-·Ar in the region of the ν_3 frequency has been reported by Relph *et al.*[48] using IR predissociation spectroscopy. We therefore explored the effect of IR excitation on the anion photoelectron spectrum with frequencies near the anion ν_3 frequency of 1349 cm^{-1} determined in that work. The top panels of Figs. 1 and 2 show overview (green) and high-resolution (black) cryo-SEVI spectra of NO_3^- out to 33000 cm^{-1} with no IR excitation. (IR on)-(IR off) photoelectron spectra for IR excitation at 1356 and 1350 cm^{-1} are shown in in the main sections of Figs. 1 and 2, respectively, and peak positions are listed in Tables 1-3. Negative-going features correspond to peaks in the ground-state photoelectron spectrum that are depleted by IR excitation, while positive-going features are from vibrationally excited anions. The two (IR on)-(IR off) spectra are clearly different, with several more peaks seen for 1350 cm^{-1} excitation (Fig. 2).

The IR off spectra in Fig. 1 are similar to those reported in Ref. 26 but yield more accurate peak positions (see Table 1), as improved signal-to-noise and reduced ion temperature enabled us to take better-resolved spectra at lower eKE. Following the assignment of Ref. 26, peaks g1, g2, and g4 are assigned to the 0_0^0, 4_0^1, and 3_0^1 transitions, respectively, keeping in mind that there is a small 1_0^1 contribution to g4. The more accurate energy for g1 yields a refined electron affinity of 31680(9) cm^{-1} for NO_3. This peak is barely visible in the high-resolution cryo-SEVI spectrum (black trace, see insert) owing to its small photodetachment cross section for slow electrons characteristic of p-wave detachment, as discussed previously.[26] Note that the eBE of the 4_0^1 peak is shifted by 364 cm^{-1} with respect to the new electron affinity value, which is in excellent agreement with the ν_4 frequency of 365.5 cm^{-1} extracted from high-resolution IR spectra.[7]

IR pre-excitation at 1356 cm^{-1} (Fig. 1) leads to depletion of the 4_0^1 feature (g2) at 32044 cm^{-1}. Depletion of the vibrational origin (0_0^0, g1) is not observed owing to its low intensity at high resolution. Many new features arise from IR excitation. Peak f1, located at an eBE of 30329(3), is shifted by -1351 cm^{-1} with respect to peak g1 in the IR off spectrum, which is approximately equal to the IR excitation energy and implies that f1 is the 3_1^0 transition from the anion $\nu_3 = 1$ level to the neutral ground vibrational state. Two other prominent features of comparable intensity are f3

and f7, which are shifted by 1051 cm^{-1} and 1493 cm^{-1} relative to f1, respectively, and clearly match the two potential values for the neutral ν_3 frequency that have been previously discussed in the literature. The spacing of the three peaks f1, f3, and f7 is the same as the previously assigned 0_0^0, 3_0^1, and $3_0^1 4_0^1(e')$ peaks in the ground state cryo-SEVI spectrum of NO_3^-.[26] This correspondence suggests that peaks f3 and f7 can be assigned to the 3_1^1 and $3_1^1 4_0^1(e')$ transitions, respectively. These assignments are discussed in more detail in Section 4.3; one key point of the analysis is that f3 actually comprises the two closely spaced 3_1^1 and $3_1^0 1_0^1$ transitions with comparable intensities.

Despite the small difference in the IR excitation frequency, pre-excitation at 1350 cm^{-1} (Fig. 2) yields a markedly different spectrum compared to 1356 cm^{-1}. All features that are observed in Fig. 1 also appear in Fig. 2 with similar intensity ratios and are therefore labeled f1-f10 in the same manner. However, a set of additional features o1-o12 appear at eBE values below and above feature f1. Since f1 is assigned to a transition into the neutral ground state (i.e., 3_1^0), a one-photon IR excitation cannot lead to peaks with eBE values lower than that of f1; despite this, peak o4 has a lower eBE, 30031 cm^{-1}, and is the most intense peak among the additional features in Fig. 2. Note that peak o4 is shifted by -1349 cm^{-1} with respect to peak f3, corresponding almost exactly to the IR excitation frequency. Our assignment of peak f3 to the 3_1^1 transition then implies that peak o4 is the 3_2^1 transition. This transition could be seen if IR excitation at 1350 cm^{-1} accesses one of the $\nu_3 = 2$ states of NO_3^- by a two-photon transition, as illustrated in the inset of Fig. 3. The assignment of peak o4 to the 3_2^1 transition is a critical aspect of this work and is explored further in Section 4.3.

Further insight into the two different IR excitation cases is obtained by measuring IR action spectra of the anion in the region 1340-1360 cm^{-1} for multiple features of the photodetachment spectra. Fig. 3 shows the depletion action spectrum of the 4_0^1 peak (black dots) and the growth spectra of peaks f1 and o4 (blue and red dots, respectively). The depletion and f1 growth spectra are essentially identical, whereas the o4 growth spectrum is narrower, lining up with the low frequency edge of the depletion spectrum but dropping noticeably above 1354 cm^{-1}. These results are consistent with the energy level scheme shown in the inset of Fig. 3, in which IR light at 1356 cm^{-1} excites the anion ν_3 fundamental while at 1350 cm^{-1}, the $\nu_3 = 2$ anion state is additionally excited by a resonant two-photon process through the $\nu_3 = 1$ state. Using PGOPHER,[58] a vibrational band center of 1350.5 cm^{-1} and an ion temperature of ~12 K can be extracted from the IR action spectra

for the ν_3 fundamental (see Fig. S1). The narrower, red-shifted profile of the o4 action spectrum is consistent with the requirement that the IR light must be resonant both with the anion $\nu_3 = 1 \leftarrow 0$ and $2 \leftarrow 1$ transitions and the expected anharmonicity of the anion ν_3 mode, leading to the conclusion that the $2\nu_3$ level must be located just slightly below 2700 cm^{-1}. At 1356 cm^{-1}, the IR light is no longer resonant with both transitions and only excitation of the anion fundamental occurs. By reducing the IR laser power at 1350 cm^{-1} from 500 to 150 µJ/pulse in a test measurement, the photodetachment peaks related to $2\nu_3$ excitation are almost completely suppressed and the IR on spectrum resembles that taken at 1356 cm^{-1}, consistent with the assumption that these features arise from a two-photon process.

As mentioned above, features, f1, f3, and o4 are distinct and show large intensities and frequency shifts that appear to be connected to the proposed ν_3 frequencies in the anion and neutral. Photoelectron spectra of those peaks were therefore measured at the highest possible resolution, using detachment energies only 20-30 cm^{-1} higher than the respective peak centers, as presented in Fig. S2. All three peaks show appreciable electron signal at these small eKE values, indicating that they result from s-wave detachment. For excitation at 1350 cm^{-1} (black curves), the profiles are symmetric and have the same shape and width for each peak. From Gaussian fits, a FWHM of 7 cm^{-1} is determined for each peak, as listed in Tables 1-3, implying that each of these peaks consists of a single peak or an unresolved doublet with a peak separation of less than 7 cm^{-1}. For excitation at 1356 cm^{-1} (red curves), asymmetric peak shapes of comparable width are observed that also appear to be identical for each transition and represent unresolved rotational structure.

Fig. 4 shows the anisotropy parameters as a function of eKE for the same selected transitions involving the ν_3 mode that were extracted from the IR-cryo-SEVI spectra. These are compared with anisotropy parameter curves of the 0_0^0 and 4_0^1 transitions measured by Babin *et al.*[26] The two curves for these transitions from the anion ground-state (a_1' symmetry) represent the two limiting cases of a FC-allowed transition (0_0^0 ends up in a final state of a_1' symmetry) and transitions induced by pJT coupling (4_0^1 ends up in a final state of e' symmetry), respectively. As already noted in Ref. 26, the 0_0^0 and 4_0^1 transitions show completely different anisotropy parameter curves with opposite signs for β at all finite eKE values, making them easily distinguishable.

It is immediately clear that all transitions extracted from the IR-cryo-SEVI spectra shown in Fig. 4 are similar to the 4_0^1 curve and do not follow the 0_0^0 curve, indicating a major vibronic contribution

over the whole eKE range covered here, which is also consistent with the interpretation that these features result from s-wave detachment. We interpret the subtle deviation of the curve for peak f3, which is reflected in consistently more positive β values than those of the 3_1^0 and 3_2^1 transitions at eKE values above ~1000 cm^{-1}, as an increasing FC contribution this peak. This trend is consistent with assigning peak f3 to a mixed $3_1^1/3_1^0 1_0^1$ transition, as discussed in more detail in Section 4.3.1. Note that essentially all newly observed IR-cryo-SEVI transitions, even those not explicitly shown in Fig. 4, show negative β values at eKE values larger than 50-100 cm^{-1}. This result clearly highlights the dominant role vibronic contributions play in the photoelectron spectra of vibrationally excited NO_3^- from an experimental standpoint.

4.2. Simulated photoelectron spectra using the Köppel-Domcke-Cederbaum Hamiltonian

Before discussing the assignment of the features observed in the IR-cryo-SEVI spectra of Figs. 1 and 2, the experimental spectra for a selected detachment energy of 32168 cm^{-1} will be compared to simulated spectra obtained with the KDC Hamiltonian (see Section 3 for details). This vibronic Hamiltonian has been used previously to successfully reproduce other nitrate spectra, including anion photoelectron[26] and LIF spectra.[55]

Figs. 5 and 6 compare the experimental spectrum for ν_3 and $2\nu_3$ excitation, respectively, with two types of simulated photoelectron spectra originating from the same anion states. For the first type of simulation (middle panel), only the photodetachment transition moment into the $\tilde{B}$ state contributes while the transition moment into the $\tilde{X}$ state is set to 0. For the second type of simulation (bottom panel) a 1/100 times smaller transition moment for the $\tilde{X}$ state compared to the $\tilde{B}$ state is assumed and the transition moment into the $\tilde{B}$ state is set to 0 – effectively showing only the $\tilde{X}$ state contribution. To a good approximation, the $\tilde{X}$ state simulation reproduces the FC-allowed features in the spectrum, while the $\tilde{B}$ state simulation yields transitions allowed via pJT coupling between the $\tilde{X}$ and $\tilde{B}$ states. Because interference between the two contributions is expected when transitions into the same neutral state are present in both the $\tilde{X}$ state and $\tilde{B}$ state spectra, the two contributions cannot simply be added to yield the full simulated spectrum. However, it is instructive to compare the individual simulated contributions with the experiment because they generally show different features or features of greatly differing intensity.

Overall, the $\tilde{B}$ state simulation in Fig. 5 provides a good description of the experimental spectrum for ν_3 pre-excitation at 1356 cm^{-1}. The $\tilde{X}$ state simulation, on the other hand, can only replicate feature f3 with reasonable intensity and does not explain many of the experimentally observed peaks, especially the transitions f1, f2 and f7. Note that the feature f3 comprises only a single transition in the $\tilde{X}$ state simulation but two transitions in the $\tilde{B}$ state simulation. In addition, the weak simulated peak at 30700 cm^{-1}, which is only seen in the $\tilde{X}$ state simulation, is not clearly observed in the experimental spectra at low electron kinetic energies, but does grow in at eKE values of 3000 cm^{-1} or higher (see Fig. S3).

A similar situation arises when comparing the $\tilde{B}$ and $\tilde{X}$ state simulations with the experimental spectra for IR excitation at 1350 cm^{-1} (Fig. 6), which are interpreted to result from a combination of ν_3 and $2\nu_3$ excitation in the anion. Again, the only experimental feature that is reasonably reproduced by the $\tilde{X}$ state simulation is f3. Other simulated features in the $\tilde{X}$ state simulation either show intensities that are too small or features that are not observed. The $\tilde{B}$ state simulation, however, again shows good agreement with the experiment. Note that for both simulations in Fig. 6, the relative contribution of the simulated spectrum arising from $2\nu_3$ vs. ν_3 pre-excitation is chosen such that the relative peak intensities of o4 and f1 are reproduced in the $\tilde{B}$ state simulation (0.4:1). Moreover, two of the prominent new features in the $\tilde{B}$ state simulation at low eBE (o1 and o4) both arise from a single transition each and do not appear in the $\tilde{X}$ state simulation.

4.3. Assignment

4.3.1. Assignment of the main features in the ν_3 IR-cryo-SEVI spectrum

From Section 4.2, it is clear that the $\tilde{B}$ state simulations generally give much better agreement with the experiment than the $\tilde{X}$ state simulations, meaning that an assignment based on FC factors and standard symmetry arguments typically employed to interpret cryo-SEVI spectra will not be successful in explaining the NO_3^- IR-cryo-SEVI spectra. Instead, one would expect the lowest-order vibronic coupling terms involving the ν_3 mode to be responsible for most transitions from the anion ν_3 state. Therefore, a large part of the following assignment also relies on the simulations using the vibronic KDC Hamiltonian and previously assigned vibrational frequencies in the IR and LIF spectra. All assignments for ν_3 pre-excitation can be found in Table 2.

Peak f1, which shows a shift of −1351 cm^{-1} with respect to 0_0^0 in the IR off spectrum, is clearly assigned to the 3_1^0 transition and marks the onset of the ν_3 IR-cryo-SEVI spectrum. The high intensity peaks f3 and f7 show shifts of 1051 and 1493 cm^{-1} relative to 3_1^0, respectively, and correspond to the two infamous vibrational levels that have both been assigned to the ν_3 mode of neutral NO_3 in the past.

We will first discuss peak f3. Most notably, this is the highest intensity peak next to peak f1 and the $\tilde{B}$ state simulation in Fig. 5 shows that this peak is likely composed of two different peaks at very similar frequencies, which the simulation identifies as 3_1^1 and $3_1^0 1_0^1$, with the latter having a slightly higher contribution. Here, the intensity of the $3_1^0 1_0^1$ contribution, just like the intense 3_1^0 transition, arises mainly from pJT coupling. The 3_1^1 contribution, on the other hand, arises from both vibronic and FC contributions. Because of this, the relative intensity contributions of the 3_1^1 vs. $3_1^0 1_0^1$ transitions to f3 are hard to estimate without knowing the exact cross section ratio $\sigma_{\tilde{X}}/\sigma_{\tilde{B}}$ in this eKE regime. Based on the good agreement between the experiment and the $\tilde{B}$ state simulation, we do however speculate that the $\tilde{X}$ state contribution to 3_1^1 only modulates the overall f3 peak intensity, which is then mainly determined by its $\tilde{B}$ state contributions. This proposed doublet structure of peak f3 could not be resolved even at the highest resolution IR-cryo-SEVI spectrum (FWHM ~7 cm^{-1}, see Fig. S2). However, the anisotropy parameter curve for peak f3 (Fig. 4), which mostly follows that of a vibronically allowed transition and slightly deviates at higher eKE, is completely consistent with this interpretation. A more detailed discussion of the vibronic coupling mechanisms that are responsible for the intensities of 3_1^0, 3_1^1 and $3_1^0 1_0^1$ can be found in Section 5.

Having assigned peak f3 to a doublet consisting of 3_1^1 and $3_1^0 1_0^1$, this leaves us with $3_1^1 4_0^1$ as the assignment for the other intense peak f7 at a shift of 1493 cm^{-1}, the level that had been originally assigned to the ν_3 level by Hirota and co-workers.[3, 13] Note, however, that only the $\nu_3 + \nu_4(e')$ component of this combination band in the neutral has high intensity in the $\tilde{B}$ state simulation of Fig. 5. Assignments of the remaining lower intensity peaks are discussed in Section 4.3.3.

4.3.2. Assignment of the main features in the $2\nu_3(e')$ IR-cryo-SEVI spectrum

Our assignment of peak f3 to a doublet comprising the $3_1^0 1_0^1$ and 3_1^1 transition places the neutral ν_3 frequency at 1051 cm^{-1}, i.e., the spacing between peaks f1 and f3. However, given the history of

NO_3 spectroscopy, one would like to assign this frequency based on an unblended peak; the $2\nu_3(e')$ overtone spectrum in Fig. 2 offers an opportunity to do this. All assignments for the $2\nu_3(e')$ spectrum can be found in Table 3.

Comparing the experimental spectrum with the $\tilde{B}$ state simulation in Fig. 6, there is little doubt that the observed spectrum indeed results from a mixture of the previously discussed ν_3 spectrum and an $2\nu_3(e')$ overtone spectrum. To exclude the possibility that excitation of the nearby $2\nu_3(a_1')$ level could lead to an alternative interpretation, we performed accurate vibrational frequency calculations for the NO_3^- anion as outlined in the SI (also see Table S1). The anharmonic frequency calculations for the anion predict a ν_3 frequency of 1351 cm^{-1}, in good agreement with the vibrational band center of 1350.5 cm^{-1} extracted from the IR action spectra. The $2\nu_3(a_1')$ and $2\nu_3(e')$ anion frequencies are calculated as 2679 and 2700 cm^{-1}, respectively. Considering the excellent accuracy of the calculations for the ν_3 level, pre-excitation of the $2\nu_3(e')$ overtone level at $\tilde{\nu}_{\mathrm{IR}} = 1350$ cm^{-1} is therefore more likely. Nevertheless, the simulated spectrum for $2\nu_3(a_1')$ excitation is presented in Fig. S4 and shows only minor differences compared to the $2\nu_3(e')$ simulation in Fig. 6. Therefore, only the $2\nu_3(e')$ spectrum is discussed in the following.

With the refined electron affinity (i.e., the eBE of the 0_0^0 transition at $EA = 31680$ cm^{-1}) extracted from the IR off spectra and the excitation energy determined by the 1+1 photon excitation ($2\tilde{\nu}_{IR} =$ 2×1350 cm^{-1}), we obtain a relatively accurate estimate of the expected eBE for the 3_2^0 transition, which should appear at around $EA - 2\tilde{\nu}_{IR} = 28980$ cm^{-1}. Clearly, the 3_2^0 transition is not observed at this eBE value for any of the detachment energies used in Fig. 2, an important observation for the following discussion. However, based on this estimate we can readily assign peak o1 to $3_2^0 4_0^1$, as it shows a shift of 372 cm^{-1} with respect to $EA - 2\tilde{\nu}_{IR}$, which further validates the accuracy of this estimate and allows us to deduce the neutral energy level positions for all peaks in the overtone spectrum.

The most intense peak (o4) shows a shift of 1051 cm^{-1} with respect to $EA - 2\tilde{\nu}_{IR}$, which is basically identical with the shift observed for $3_1^1/3_1^0 1_0^1$ (f3) with respect to the 3_1^0 (f1) transition. This leaves only two options for the final neutral level, either ν_1 or ν_3. The choice of assigning o4 to 3_2^1 over $3_2^0 1_0^1$ is not only the simplest choice for the assignment, involving only a single-quanta change rather than a three-quanta change, but it also appears to be the most reasonable choice when considering the changes in quantum numbers ν_1 and ν_3 individually. With $\Delta\nu_3 = -1$, the intense

3_2^1 transition can be considered analogous to the 3_1^0 transition, the latter being the most intense transition in the fundamental excitation spectrum. However, the most convincing argument for 3_2^1 over $3_2^0 1_0^1$ is that the 3_2^0 transition is clearly not observed in any of the experimental spectra in Fig. 2. If a $3_2^0 1_0^1$ contribution was present, the 3_2^0 transition—differing only in the additional excitation of the totally symmetric and nominally FC-active ν_1 mode—should also be observed. Furthermore, it should be observed with a relative intensity that approximately reflects the ratio between the FC factors of 1_0^1 and 0_0^0 in the ground-state cryo-SEVI spectrum. However, the ratio for 1_0^1 vs. 0_0^0 is around 1:8, as apparent from the simulation of the cryo-SEVI spectrum in Fig. 2 of Ref. 26, indicating that the intensity of the $3_2^0 1_0^1$ should be about 8 times lower compared to 3_2^0. We attribute the vanishing intensity in the 3_2^0 transition to the fact that the zeroth-order vibronic $\tilde{X}\ ^2A_2'(v=0)$ and $\tilde{B}\ ^2E'(2\nu_3)$ levels cannot efficiently be coupled by first-order vibronic interactions, which is explained in more detail in Section 5. Considering all this evidence, it is probably not surprising that the $\tilde{B}$ state simulation in Fig. 6 shows the contribution of only a single transition to peak o4, which is assigned to 3_2^1. This places the neutral ν_3 frequency at 1051 cm^{-1} and the assignment of o4 to 3_2^1 will be further discussed in Section 5.

The only other low-frequency vibration observed in the overtone spectrum in Fig. 6 is associated with peak o5 at a shift of 1492 cm^{-1}, which is assigned to the $3_2^1 4_0^1(e')$ transition by comparison with the KDC simulation. This transition involves an additional $\Delta v_4 = 1$ quanta change and only gains significant intensity for higher photodetachment energies, as seen for example in Fig. 2, indicating p-wave detachment and a FC contribution, which would not be expected for 3_2^1. Therefore, the result that o5 shows significantly less intensity than o4 is completely consistent with their assignments to $3_2^1 4_0^1(e')$ and 3_2^1, respectively.

4.3.3. Remaining assignments in the ν_3 and $2\nu_3$ IR-cryo-SEVI spectra

Assignments of the remaining features in Figs. 1 and 2 are discussed here. The order of the discussed features will approximately follow the order of the corresponding neutral level energies in Tables 2 and 3, respectively.

A pure ν_4 progression can be observed in the ν_3 IR-cryo-SEVI spectra in Fig. 1. The first feature of this progression is f2, which is assigned to $3_1^0 4_0^2$. Known IR frequencies of $2\nu_4(a_1')$ and $2\nu_4(e')$, are 752 and 772 cm^{-1}, respectively,[7, 9] and the peak position of f2 suggests that the main

contribution originates from the $2\nu_4(e')$ level, consistent with the simulation. The next observed peak within this ν_4 progression, f4, is assigned to $3_1^0 4_0^3(e')$, as this is the only $3_1^0 4_0^3$ state in the simulated $\tilde{B}$ state spectrum of Fig. 5 and agrees with Kawaguchi's assignment. The $3_1^0 4_0^1$ transition, expected at about 30700 cm^{-1} according to the $\tilde{X}$ state simulation, is not clearly observed until the eKE of this peak exceeds ~3000 cm^{-1} (see Fig. S3). This indicates that $3_1^0 4_0^1$ is FC- but not vibronically allowed, consistent with its appearance in the $\tilde{X}$ but not the $\tilde{B}$ state simulation.

Peak f5 is assigned to another $3_1^1 4_0^1$ state of a_2' symmetry that appears at much lower eBE than the $3_1^1 4_0^1(e')$ component (f7), as its experimental shift of 1364 cm^{-1} to 3_1^0 is close to that predicted by the KDC simulation. This level has not been experimentally observed to our knowledge but is predicted at a similar energy (1330 cm^{-1}) in calculations using coupled diabatic potential energy surfaces.[59] The location of $\nu_3 + \nu_4(a_2')$ far below the other $\nu_3 + \nu_4$ states near 1490 cm^{-1} may explain why only a single $\nu_3 + \nu_4 \leftarrow \nu_4$ hot band of a symmetry has been observed with IR spectroscopy in prior work.[8, 36] The nearby peak f6 is consistent with the $3_1^0 1_0^1 4_0^1$ transition seen in the simulation and its position agrees well with the IR frequency of 1413.6 cm^{-1} for the $\nu_1 + \nu_4$ combination band.[10] Finally, peak f8 can be assigned to the $3_1^1 4_0^2(e')$ transition by comparison with the KDC simulation. The shift of 1774 cm^{-1} greatly differs from the IR frequency proposed by Kawaguchi and co-workers (1950 cm^{-1}),[9] which was however not directly measured and only inferred using a simple vibronic interaction model to describe nearby states.

The accuracy of the KDC simulations starts deteriorating above 2000 cm^{-1}. However, despite the limited predictability in this range, peaks o6 and o7 (Fig. 2) as well as peaks f9 and f10 (Fig. 1) can still be assigned based on previous IR experiments and deserve special attention, as they seem to correspond to the same vibrational levels (as reflected in similar shifts to 3_2^0 and 3_1^0, respectively) and each pair shows a similar intensity ratio. The neutral energy levels line up with the IR transitions at 2024.3 and 2155.0 cm^{-1} reported by Kawaguchi *et al.*[10, 12] Based on the anharmonicity analysis carried out in Ref. 12, these levels carry dominant $\nu_1 + \nu_3$ and $2\nu_3(e')$ character, respectively. Another IR-active state at 2205.7 cm^{-1} is also strongly mixed with these two levels and has dominant $\nu_1 + 3\nu_4\ (e')$ character.[12] Peak o8 in the $2\nu_3$ IR-cryo-SEVI is consistent with this third state at 2205.7 cm^{-1} , but only appears at higher eKE following p-wave detachment, indicating a stronger FC contribution compared to o6 and o7. The equivalent peak in the ν_3 IR-cryo-SEVI spectra cannot be observed in Fig. 1; however, it appears as a shoulder at much higher

photon energies at an eBE of around 32520 cm^{-1} in Fig. S3. According to the analysis of Kawaguchi *et al.*,[12] the mixing between those three states is so strong that an individual assignment may not be an appropriate description. Since the $2\nu_3(e')$ character of these states must be at least partially responsible for the photodetachment intensities into these states, we will collectively refer to these states as a $2\nu_3(e')$ polyad.

While the basic structure of this polyad can be seen in the KDC simulations in Fig. 6 between 31000 and 31200 cm^{-1}, the experimental position of o6 is not reproduced. This can likely be attributed to the declining accuracy of the KDC simulations above 2000 cm^{-1}. The simulated positions of the polyad features should also critically depend on the close spacing between the ν_1 and ν_3 fundamental frequencies (~4 cm^{-1}), which is not quantitatively captured by the KDC Hamiltonian. Whereas in the fundamental region, the two vibrations cannot interact because of differing symmetries, in the overtone region, a strong interaction results for the $\nu_1 + \nu_3(e')$ and $2\nu_3(e')$ combination band and overtone.

The low intensity features o2 and o3 appear in a region where only $3_2^0 4_0^2$ transitions would be expected. However, the position of o2 is not consistent with the well-known $2\nu_4(a_1')$ and $2\nu_4(e')$ frequencies of 752 and 772 cm^{-1}, respectively.[7, 9] It is therefore possible that peaks o2 and o3 arise from $3\nu_3$ excitation in the anion, specifically the levels of a_1' and a_2' vibrational symmetry, which according to the anharmonic frequency calculations in Table S1 are also accessible at an IR frequency of 1350 cm^{-1} from the $2\nu_3(e')$ state via absorption of an additional photon. Under this assumption, the shifts of o2 and o3 to $EA - 3 \times \tilde{\nu}_{IR}$, respectively, would be 2030 cm^{-1} and 2160 cm^{-1}, in close agreement with two of the $2\nu_3(e')$ polyad levels discussed above. However, given their low intensities, no definite assignment can be made.

Features o9-o12 correspond to neutral levels with energies above 2600 cm^{-1}. Features o9, o11 and o12 are thus left unassigned. Although rough predictions in this energy range exist from IR experiments[10] and recent calculations,[59] there are too many potential candidate states. Without a prediction of the photodetachment spectrum using the KDC Hamiltonian, no reasonable assignment can be made. Peak o10, which is prominently featured in the $2\nu_3$ IR cyo-SEVI spectrum, presents an exception. It is assigned to a $3_1^1 1_0^1 4_0^2(e')$ transition based on the intense, assigned IR transition observed at a frequency matching 2902 cm^{-1}.[10]

5. Discussion

Considering the history of the discussion centered around the correct assignment of the ν_3 frequency and the fact that most other frequencies below 2000 cm^{-1} have already been unambiguously assigned in the past, we will focus on a few points that provide extremely strong evidence that peak o4 can only be assigned to a 3_2^1 transition from the excited $2\nu_3(e')$ overtone anion level into the ν_3 level of the neutral, thereby placing the ν_3 frequency at ~1050 cm^{-1}.

An important point to consider is the prevalence of transitions that are nominally not FC-allowed, which becomes apparent from a comparison of the experimental spectra to the contribution of the $\tilde{B}$ state vs. that of the $\tilde{X}$ state in Figs. 5 and 6. Clearly, little agreement with the $\tilde{X}$ state contributions can be observed for most peaks, except the FC-allowed contribution to 3_1^1. This is supported by the observation that essentially all transitions originating from vibrationally excited NO_3^- show negative anisotropy parameters, consistent with those expected for a transition gaining intensity from the $\tilde{B}$ state. In fact, such an observation is expected given that most transitions starting from an excited ν_3 or $2\nu_3$ level involve a one- or two-quanta change in the ν_3 mode, a stretching vibration for which FC activity is not normally seen.[47]

As a consequence, the strong 3_1^0 and 3_2^1 transitions solely result from pJT coupling between the corresponding $\tilde{X}\ ^2A_2'$ and $\tilde{B}\ ^2E'$ levels as reflected in the simulations in Figs. 5 and 6, respectively. In the case of 3_1^0, the reason is the strong pJT interaction between the vibronic $\tilde{X}\ ^2A_2'(v=0)$ and $\tilde{B}\ ^2E'(\nu_3)$ zeroth-order states, where the latter state is expected to show strong overlap with the initial $\tilde{X}\ ^1A_1'(\nu_3)$ anion state. Similarly, 3_2^1 gains most intensity through a pJT interaction between the $\tilde{X}\ ^2A_2'(\nu_3)$ and $\tilde{B}\ ^2E'(2\nu_3)$ zeroth-order states, where the latter has overlap with the excited $\tilde{X}\ ^1A_1'(2\nu_3)$ anion state. It is important to realize that 3_2^0, whose observation would be the prerequisite for observing any potential $3_2^0 1_0^1$ contribution, as discussed above, does not gain intensity through this simple mechanism involving only the linear pJT coupling term, as it only couples vibronic levels that differ by $\Delta v_3 = 1$. Therefore, the vibronic $\tilde{X}\ ^2A_2'(v=0)$ and $\tilde{B}\ ^2E'(2\nu_3)$ zeroth-order states do not show efficient mixing, explaining the vanishingly small intensity for the 3_2^0 and $3_2^0 1_0^1$ transitions in stark contrast to 3_1^0 and 3_2^1.

In a similar manner, we can also qualitatively rationalize the small $\tilde{B}$ state contribution to the 3_1^1 transition seen in Fig. 5. However, in this case JT coupling within the $\tilde{B}$ state needs to be considered

in addition to pJT coupling between the $\tilde{X}$ and $\tilde{B}$ states. The vibronic $\tilde{B}\ ^2E'(\nu_3)$ zeroth-order state, which is accessible from the $\tilde{X}\ ^1A_1'(\nu_3)$ anion state, can couple to $\tilde{B}\ ^2E'(v=0)$ or $\tilde{B}\ ^2E'(2\nu_3)$, which in turn are coupled to the $\tilde{X}\ ^2A_2'(\nu_3)$ zeroth-order state via pJT interactions. In addition, other pathways based on higher-order JT coupling terms likely contribute to the vibronic part of the 3_1^1 intensity.

Finally, recently published LIF spectra of NO_3 show two vibrational modes with band centers at 1051 and 1055 cm^{-1}.[18] The former can clearly be assigned to ν_1, as its position barely changes upon ^{15}N substitution; the latter must then be assigned to ν_3 based on the IR-cryo-SEVI results presented in this work. This ν_3 position is consistent with the vibrational level at 1054.1 cm^{-1} that Kawaguchi *et al.* derived from extremely weak rovibrational lines observed with IR spectroscopy and which they assigned to the ν_3 fundamental.[11] Additionally, the alternative assignment of the 1055 cm^{-1} feature to $3\nu_4(a_1')$ instead of ν_3, which is given in Ref. 18, can easily be ruled out by comparison to the surrounding features in the LIF spectra, which are assigned to the $n\nu_4$ progression. The intensity of the $3\nu_4(a_1')$ transition is higher in intensity by about a factor of five compared to all other features in this progression and its position would indicate a fairly large splitting of more than 100 cm^{-1} between the $3\nu_4(a_1')$ and the other $3\nu_4$ levels. We also point out that the assignment of the 1055 cm^{-1} peak to ν_3 is consistent with the simulation of the LIF spectrum based on the same vibronic Hamiltonian used in the present work.[55]

Considering the observation of peak o4 with its dominant contribution to the $2\nu_3$ IR-cryo-SEVI spectrum and the discussion above, there appears to be no option other than assigning this feature to the 3_2^1 transition. From its binding energy at 30031 cm^{-1}, the electron affinity (i.e., the binding energy of 0_0^0) of 31680 cm^{-1} and the IR excitation frequency of 2×1350 cm^{-1} for $2\nu_3$, we therefore extract a ν_3 fundamental frequency of the neutral of 1051 cm^{-1}. The error of this estimate is largely dependent on the accuracy of the eBE of the 0_0^0 transition, which occurs via p-wave detachment and can only be measured with a 1σ width of 9 cm^{-1} that results from the relatively large eKE needed to observe it with appreciable intensity. However, a more accurate estimate of the neutral ν_3 frequency from the IR-cryo-SEVI spectra can be made based on the $3_1^0 1_0^1/3_1^1$ doublet that constitutes peak f3, even though this peak is not resolved. Because of the symmetric peak shapes and narrow widths in the $2\nu_3$ IR-cryo-SEVI spectra (see Fig. S2), we assume that the error in determining the each of the two peak positions is mainly limited by the ~3 cm^{-1} accuracy of the

eKE calibration. The difference in binding energies between peak f1 (the 3_1^0 transition) and f3 (containing the 3_1^1 transition) is therefore determined as 1051±4 cm^{-1} and serves as a more accurate estimate of the ν_3 fundamental frequency based on our experiments.

6. Conclusion

High-resolution photoelectron spectra as well as IR action spectra for both ν_3 and $2\nu_3$ IR pre-excitation of the NO_3^- anion have been presented. By selectively monitoring photoelectron peaks that arise from ν_3 excitation, we obtain an estimate of 1350.5 cm^{-1} for the ν_3 frequency of the anion. The overtone pre-excitation becomes possible through a resonant 1+1 photon process that is most efficient at an IR frequency near 1350 cm^{-1} and results from the fact that the $2\nu_3(e')$ anion level lies close to twice the energy of the ν_3 fundamental at ~2700 cm^{-1}, which is further confirmed by accurate anharmonic frequency computations. Careful selection of the IR excitation frequency thus enables us to selectively observe photoelectron spectra in which either the ν_3 fundamental or both the ν_3 fundamental and $2\nu_3(e')$ overtone are excited.

Most importantly, the $2\nu_3$ IR-cryo-SEVI spectrum shows an intense transition at 30031 cm^{-1} that can only be assigned to the 3_2^1 transition. From this transition, as well the difference between the 3_1^0 transition and the unresolved $3_1^0 1_0^1/3_1^1$ transitions observed in the ν_3 IR-cryo-SEVI spectrum, the ν_3 frequency of the NO_3 radical is determined as 1051±4 cm^{-1}. The large intensity of the 3_2^1 transition is explained by pseudo Jahn-Teller coupling that efficiently mixes the contributions of the vibronic $\tilde{X}\ ^2A_2'(\nu_3)$ and $\tilde{B}\ ^2E'(2\nu_3)$ zeroth-order states through a first-order coupling term, where the latter state has strong overlap with the prepared anion vibrational state. The same mechanism is not possible for the 3_2^0 and $3_2^0 1_0^1$ transitions, which is the main reason they are not observed experimentally.

Consideration of vibronic coupling is extremely important for explaining the observed intensities in the photodetachment spectra of vibrationally excited NO_3^-. This is confirmed experimentally by negative anisotropy parameters and large intensities at low electron kinetic energies below ~3000 cm^{-1} observed for essentially all transitions arising from IR pre-excitation. The importance of vibronic coupling is further confirmed by a comparison with simulations based on a vibronic Köppel-Domcke-Cederbaum Hamiltonian, in which contributions from the $\tilde{X}\ ^2A_2'$ and $\tilde{B}\ ^2E'$

diabatic states are considered separately. Only the spectra based on the $\tilde{B}$ state contribution provide an adequate description of the experimentally observed spectra. Of the higher intensity photodetachment features, only the 3_1^1 transition shows a significant Franck-Condon contribution that originates from the $\tilde{X}$ state, as expected for a stretching vibration. Without the inclusion of pJT coupling to the $\tilde{B}$ state, however, barely any of the experimentally observed IR-cryo-SEVI features would be reproduced.

With regards to the controversy that surrounds the position of the ν_3 fundamental level of NO_3, the results of this study are unequivocal. It is located near 1054 cm^{-1}, first resolved (and misassigned) by Fukushima using high-resolution laser-induced fluorescence from the $\tilde{B}\ ^2E'$ origin,[18] and later by direct absorption in the infrared by Kawaguchi (which was correctly assigned), the latter obtaining a precise position of 1054.1 cm^{-1}.[11] The present work makes it abundantly clear that this level (observed here in somewhat lower resolution) is indeed the ν_3 fundamental. This is particularly demonstrated in the combined and detailed analysis of the spectra associated with the anion vibrational ground state as well as its ν_3 fundamental and overtone levels. Aided by simulations of the spectrum, a fully self-consistent interpretation of the experimental results has been achieved.

Indeed, the confirmation of what has been called ‘‘Assignment B’’ (with the historically accepted “Assignment A” placing ν_3 at 1492 cm^{-1}) in this work should be regarded as setting a standard of rigor. In order to be regarded seriously, any further works arguing for the historical assignment must successfully address and refute the conclusions of this paper.

Acknowledgments

The research at U.C. Berkeley was funded by the Air Force Office of Scientific Research (AFOSR) under Grant no. FA9550-23-1-0545 and the AFOSR Defense University Research Instrumentation Program under Grant no. FA9550-19-1-0139, DEF. Research at the University of Florida was supported by the U.S. Department of Energy, Office of Basic Energy Sciences under Award DE-SC0018164. J.A.L. greatly appreciates support by the Alexander von Humboldt Foundation through a Feodor Lynen Research Fellowship.

Supporting Information

Description of anharmonic frequency calculations for NO_3^-; calculated anharmonic frequencies of NO_3^-; PGOPHER simulation of the ν_3 IR action spectrum; high-resolution IR-cryo-SEVI spectra of peaks o4, f1 and f3; IR-cryo-SEVI spectra at higher photon energies; simulated photodetachment spectra for $2\nu_3(a_1')$ pre-excitation (PDF).

References

(1) Monks, P. S. Gas-Phase Radical Chemistry in the Troposphere. *Chem. Soc. Rev.* **2005**, *34*, 376-395. DOI: 10.1039/B307982C.
(2) Chappuis, J. Étude Spectroscopique Sur L'ozone. *Annales scientifiques de l'École Normale Supérieure* **1882**, *11*, 137-186. DOI: 10.24033/asens.213.
(3) Ishiwata, T.; Tanaka, I.; Kawaguchi, K.; Hirota, E. Infrared Diode Laser Spectroscopy of the NO_3 ν_3 Band. *J. Chem. Phys.* **1985**, *82*, 2196-2205. DOI: 10.1063/1.448362.
(4) Friedl, R. R.; Sander, S. P. Fourier Transform Infrared Spectroscopy of the NO_3 ν_2 and ν_3 Bands: Absolute Line Strength Measurements. *J. Phys. Chem.* **1987**, *91*, 2721-2726. DOI: 10.1021/j100295a015.
(5) Kawaguchi, K.; Hirota, E.; Ishiwata, T.; Tanaka, I. A Reinvestigation of the NO_3 1492 cm^{-1} Band. *J. Chem. Phys.* **1990**, *93*, 951-956. DOI: 10.1063/1.459121.
(6) Kawaguchi, K.; Shimizu, N.; Fujimori, R.; Tang, J.; Ishiwata, T.; Tanaka, I. Fourier Transform Infrared Spectroscopy of the ν_3 Hot Band of NO_3. *J. Mol. Spectrosc.* **2011**, *268*, 85-92. DOI: 10.1016/j.jms.2011.04.003.
(7) Fujimori, R.; Shimizu, N.; Tang, J.; Ishiwata, T.; Kawaguchi, K. Fourier Transform Infrared Spectroscopy of the ν_2 and ν_4 Bands of NO_3. *J. Mol. Spectrosc.* **2013**, *283*, 10-17. DOI: 10.1016/j.jms.2012.11.005.
(8) Kawaguchi, K.; Fujimori, R.; Tang, J.; Ishiwata, T. FTIR Spectroscopy of NO_3: Perturbation Analysis of the ν_3+ν_4 State. *J. Phys. Chem. A* **2013**, *117*, 13732-13742. DOI: 10.1021/jp407822g.
(9) Kawaguchi, K.; Narahara, T.; Fujimori, R.; Tang, J.; Ishiwata, T. Infrared Spectroscopy of $2\nu_4$ and ν_3+$2\nu_4$ Bands of the NO_3 Radical. *J. Mol. Spectrosc.* **2017**, *334*, 10-21. DOI: 10.1016/j.jms.2017.02.008.
(10) Kawaguchi, K.; Fujimori, R.; Tang, J.; Ishiwata, T. Infrared Spectroscopy of the NO_3 Radical from 2000 to 3000 cm^{-1}. *J. Mol. Spectrosc.* **2018**, *344*, 6-16. DOI: 10.1016/j.jms.2017.09.012.
(11) Kawaguchi, K.; Tang, J.; Akikusa, N. Infrared Laser Spectroscopy of the ν_3-ν_4 Difference Band and Detection of the ν_3 Band of NO_3. *Chem. Phys. Lett.* **2021**, *765*, 138315. DOI: 10.1016/j.cplett.2020.138315.
(12) Kawaguchi, K.; Fujimori, R.; Tang, J.; Ishiwata, T. Infrared Spectroscopy of Difference and Combination Bands of the NO_3 Radical and Anharmonicity Analysis. *J. Mol. Spectrosc.* **2022**, *385*, 111594. DOI: 10.1016/j.jms.2022.111594.
(13) Ishiwata, T.; Fujiwara, I.; Naruge, Y.; Obi, K.; Tanaka, I. Study of NO_3 by Laser-Induced Fluorescence. *J. Phys. Chem.* **1983**, *87*, 1349-1352. DOI: 10.1021/j100231a016.
(14) Nelson, H. H.; Pasternack, L.; McDonald, J. R. Excited State Dynamics of NO_3. *J. Chem. Phys.* **1983**, *79*, 4279-4284. DOI: 10.1063/1.446354.
(15) Nelson, H. H.; Pasternack, L.; McDonald, J. R. Laser-Induced Excitation and Emission Spectra of NO_3. *J. Phys. Chem.* **1983**, *87*, 1286-1288. DOI: 10.1021/j100231a003.
(16) Kim, B.; Hunter, P. L.; Johnston, H. S. NO_3 Radical Studied by Laser-Induced Fluorescence. *J. Chem. Phys.* **1992**, *96*, 4057-4067. DOI: 10.1063/1.461861.

(17) Tada, K.; Kashihara, W.; Baba, M.; Ishiwata, T.; Hirota, E.; Kasahara, S. High-Resolution Laser Spectroscopy and Magnetic Effect of the $\tilde{B}\ ^2E' \leftarrow \tilde{X}\ ^2A_2'$ Transition of $^{14}NO_3$ Radical. *J. Chem. Phys.* **2014**, *141*. DOI: 10.1063/1.4901019.
(18) Fukushima, M. Laser Induced Fluorescence Spectra of the $\tilde{B}\ ^2E' - \tilde{X}\ ^2A_2'$ Transition of Jet Cooled $^{14}NO_3$ and $^{15}NO_3$ I: ν_4 Progressions in the Ground $\tilde{X}\ ^2A_2'$ State. *J. Mol. Spectrosc.* **2022**, *387*, 111646. DOI: 10.1016/j.jms.2022.111646.
(19) Fukushima, M. Laser Induced Fluorescence Spectroscopy of the Transition of Jet Cooled $^{14}NO_3$ and $^{15}NO_3$ II: The Dispersed Fluorescence Spectrum from the 3rd *E* Level of the ν_4 Mode (Approximately the $2\nu_4$ (E'), $L = 0$, Level). *Phys. Chem. Chem. Phys.* **2024**, *26*, 23307-23321. DOI: 10.1039/D4CP01719F.
(20) Deev, A.; Sommar, J.; Okumura, M. Cavity Ringdown Spectrum of the Forbidden $\tilde{A}\ ^2E'' \leftarrow \tilde{X}\ ^2A_2'$ Transition of NO_3: Evidence for Static Jahn–Teller Distortion in the Ã State. *J. Chem. Phys.* **2005**, *122*. DOI: 10.1063/1.1897364.
(21) Takematsu, K.; Eddingsaas, N. C.; Robichaud, D. J.; Okumura, M. Spectroscopic Studies of the Jahn-Teller Effect in the $\tilde{A}\ ^2E''$ State of the Nitrate Radical NO_3. *Chem. Phys. Lett.* **2013**, *555*, 57-63. DOI: 10.1016/j.cplett.2012.10.088.
(22) Codd, T.; Chen, M.-W.; Roudjane, M.; Stanton, J. F.; Miller, T. A. Jet Cooled Cavity Ringdown Spectroscopy of the $\tilde{A}\ ^2E'' \leftarrow \tilde{X}\ ^2A_2'$ Transition of the NO_3 Radical. *J. Chem. Phys.* **2015**, *142*. DOI: 10.1063/1.4919690.
(23) Jacox, M. E.; Thompson, W. E. The Infrared Spectroscopy and Photochemistry of NO_3 Trapped in Solid Neon. *J. Chem. Phys.* **2008**, *129*. DOI: 10.1063/1.3020753.
(24) Beckers, H.; Willner, H.; Jacox, M. E. Conflicting Observations Resolved by a Far IR and UV/Vis Study of the NO_3 Radical. *ChemPhysChem* **2009**, *10*, 706-710. DOI: 10.1002/cphc.200800860.
(25) Weaver, A.; Arnold, D. W.; Bradforth, S. E.; Neumark, D. M. Examination of the $^2A_2'$ and $^2E''$ States of NO_3 by Ultraviolet Photoelectron Spectroscopy of NO_3^-. *J. Chem. Phys.* **1991**, *94*, 1740-1751. DOI: 10.1063/1.459947.
(26) Babin, M. C.; DeVine, J. A.; DeWitt, M.; Stanton, J. F.; Neumark, D. M. High-Resolution Photoelectron Spectroscopy of Cryogenically Cooled NO_3^-. *J. Phys. Chem. Lett.* **2020**, *11*, 395-400. DOI: 10.1021/acs.jpclett.9b03055.
(27) Neumark, D. M. Spectroscopy of Radicals, Clusters, and Transition States Using Slow Electron Velocity-Map Imaging of Cryogenically Cooled Anions. *J. Phys. Chem. A* **2023**, *127*, 4207-4223. DOI: 10.1021/acs.jpca.3c01537.
(28) Boehm, R. C.; Lohr, L. L. An Ab Initio Characterization of Nitrogen Trioxide Electronic States. *J. Phys. Chem.* **1989**, *93*, 3430-3433. DOI: 10.1021/j100346a012.
(29) Kaldor, U. The Ground State Geometry of the NO_3 Radical. *Chem. Phys. Lett.* **1990**, *166*, 599-601. DOI: 10.1016/0009-2614(90)87156-L.
(30) Stanton, J. F.; Gauss, J.; Bartlett, R. J. On the Choice of Orbitals for Symmetry Breaking Problems with Application to NO_3. *J. Chem. Phys.* **1992**, *97*, 5554-5559. DOI: 10.1063/1.463762.
(31) Davy, R. D.; Schaefer, H. F., III. Is There an Absence of Threefold Symmetry at the Equilibrium Geometry of the Ground Electronic State for NO_3? *J. Chem. Phys.* **1989**, *91*, 4410-4411. DOI: 10.1063/1.456769.
(32) Kim, B.; Hammond, B. L.; Lester, W. A.; Johnston, H. S. Ab Initio Study of the Vibrational Spectra of NO_3. *Chem. Phys. Lett.* **1990**, *168*, 131-134. DOI: 10.1016/0009-2614(90)85117-U.
(33) Stanton, J. F.; Gauss, J.; Bartlett, R. J. Potential Nonrigidity of the NO_3 Radical. *J. Chem. Phys.* **1991**, *94*, 4084-4087. DOI: 10.1063/1.460636.

(34) Mayer, M.; Cederbaum, L. S.; Köppel, H. Ground State Dynamics of NO_3: Multimode Vibronic Borrowing Including Thermal Effects. *J. Chem. Phys.* **1994**, *100*, 899-911. DOI: 10.1063/1.466572.
(35) Stanton, J. F. On the Vibronic Level Structure in the NO_3 Radical. I. The Ground Electronic State. *J. Chem. Phys.* **2007**, *126*. DOI: 10.1063/1.2715547.
(36) Hirota, E. Vibrational Assignment and Vibronic Interaction for NO_3 in the Ground Electronic State. *J. Mol. Spectrosc.* **2015**, *310*, 99-104. DOI: 10.1016/j.jms.2014.12.010.
(37) Hirota, E. Assignment of the Photoelectron Spectrum of the Nitrate Anion NO_3^- and Vibronic Interactions in the Nitrate Free Radical. *J. Mol. Spectrosc.* **2018**, *343*, 81-84. DOI: 10.1016/j.jms.2017.11.003.
(38) F. Stanton, J. On the Vibronic Level Structure in the NO_3 Radical: II. Adiabatic Calculation of the Infrared Spectrum. *Mol. Phys.* **2009**, *107*, 1059-1075. DOI: 10.1080/00268970902740530.
(39) Viel, A.; Eisfeld, W. NO_3 Full-Dimensional Potential Energy Surfaces and Ground State Vibrational Levels Revisited. *Chem. Phys.* **2018**, *509*, 81-90. DOI: 10.1016/j.chemphys.2018.01.003.
(40) Williams, D. M. G.; Viel, A.; Eisfeld, W. Diabatic Neural Network Potentials for Accurate Vibronic Quantum Dynamics—the Test Case of Planar NO3. *J. Chem. Phys.* **2019**, *151*. DOI: 10.1063/1.5125851.
(41) Williams, D. M. G.; Eisfeld, W.; Viel, A. Simulation of the Photodetachment Spectra of the Nitrate Anion (NO_3^-) in the $\tilde{B}\ ^2E'$ Energy Range and Non-Adiabatic Electronic Population Dynamics of NO_3. *Phys. Chem. Chem. Phys.* **2022**, *24*, 24706-24713. DOI: 10.1039/D2CP02873E.
(42) Viel, A.; Williams, D. M. G.; Eisfeld, W. Accurate Quantum Dynamics Simulation of the Photodetachment Spectrum of the Nitrate Anion (NO_3^-) Based on an Artificial Neural Network Diabatic Potential Model. *J. Chem. Phys.* **2021**, *154*. DOI: 10.1063/5.0039503.
(43) Homayoon, Z.; Bowman, J. M. Communication: MULTIMODE Calculations of Low-Lying Vibrational States of NO_3 Using an Adiabatic Potential Energy Surface. *J. Chem. Phys.* **2014**, *141*. DOI: 10.1063/1.4900734.
(44) Köppel, H.; Domcke, W.; Cederbaum, L. S. Multimode Molecular Dynamics Beyond the Born-Oppenheimer Approximation. In *Advances in Chemical Physics*, 1984; pp 59-246.
(45) Wigner, E. P. On the Behavior of Cross Sections near Thresholds. *Phys. Rev.* **1948**, *73*, 1002-1009. DOI: 10.1103/PhysRev.73.1002.
(46) DeWitt, M.; Babin, M. C.; Neumark, D. M. High-Resolution Photoelectron Spectroscopy of Vibrationally Excited OH^-. *J. Phys. Chem. A* **2021**, *125*, 7260-7265. DOI: 10.1021/acs.jpca.1c05514.
(47) Lau, J. A.; DeWitt, M.; Boyer, M. A.; Babin, M. C.; Solomis, T.; Grellmann, M.; Asmis, K. R.; McCoy, A. B.; Neumark, D. M. High-Resolution Photoelectron Spectroscopy of Vibrationally Excited Vinoxide Anions. *J. Phys. Chem. A* **2023**, *127*, 3133-3147. DOI: 10.1021/acs.jpca.3c00484.
(48) Relph, R. A.; Bopp, J. C.; Johnson, M. A.; Viggiano, A. A. Argon Cluster-Mediated Isolation and Vibrational Spectra of Peroxy and Nominally D_{3h} Isomers of CO_3^- and NO_3^-. *J. Chem. Phys.* **2008**, *129*. DOI: 10.1063/1.2958223.
(49) Forney, D.; Thompson, W. E.; Jacox, M. E. The Vibrational Spectra of Molecular Ions Isolated in Solid Neon. XI. NO_2^+, NO_2^-, and NO_3^-. *J. Chem. Phys.* **1993**, *99*, 7393-7403. DOI: 10.1063/1.465720.
(50) Weichman, M. L.; DeVine, J. A.; Levine, D. S.; Kim, J. B.; Neumark, D. M. Isomer-Specific Vibronic Structure of the 9-, 1-, and 2-Anthracenyl Radicals Via Slow Photoelectron Velocity-Map Imaging. *Proc. Natl. Acad. Sci. U.S.A.* **2016**, *113*, 1698-1705. DOI: 10.1073/pnas.1520862113.

(51) DeWitt, M.; Babin, M. C.; Lau, J. A.; Solomis, T.; Neumark, D. M. High Resolution Photoelectron Spectroscopy of the Acetyl Anion. *J. Phys. Chem. A* **2022**, *126*, 7962-7970. DOI: 10.1021/acs.jpca.2c06214.
(52) Dick, B. MELEXIR: Maximum Entropy Legendre Expanded Image Reconstruction. A Fast and Efficient Method for the Analysis of Velocity Map Imaging or Photoelectron Imaging Data. *Phys. Chem. Chem. Phys.* **2019**, *21*, 19499-19512. DOI: 10.1039/c9cp03353j.
(53) Blondel, C.; Chaibi, W.; Delsart, C.; Drag, C.; Goldfarb, F.; Kröger, S. The Electron Affinities of O, Si, and S Revisited with the Photodetachment Microscope. *Eur. Phys. J. D* **2005**, *33*, 335-342. DOI: 10.1140/epjd/e2005-00069-9.
(54) Simmons, C. S.; Ichino, T.; Stanton, J. F. The ν3 Fundamental in NO3 Has Been Seen near 1060 Cm–1, Albeit Some Time Ago. *J. Phys. Chem. Lett.* **2012**, *3*, 1946-1950. DOI: 10.1021/jz300721b.
(55) Stanton, J. F. Simulation of the Dispersed Fluorescence Spectrum of the NO_3 $\tilde{B} - \tilde{X}$ Origin Vibronic Band. *J. Mol. Spectrosc.* **2022**, *389*, 111690. DOI: 10.1016/j.jms.2022.111690.
(56) Matthews, D. A.; Cheng, L.; Harding, M. E.; Lipparini, F.; Stopkowicz, S.; Jagau, T.-C.; Szalay, P. G.; Gauss, J.; Stanton, J. F. Coupled-Cluster Techniques for Computational Chemistry: The CFOUR Program Package. *J. Chem. Phys.* **2020**, *152*, 214108. DOI: 10.1063/5.0004837.
(57) Lanczos, C. An Iteration Method for the Solution of the Eigenvalue Problem of Linear Differential Equations and Integral Operators. *Journal of Research of the National Bureau of Standards* **1950**, *45*, 255-282.
(58) Western, C. M. PGOPHER: A Program for Simulating Rotational, Vibrational and Electronic Spectra. *J. Quant. Spectrosc. Radiat. Transfer* **2017**, *186*, 221-242. DOI: 10.1016/j.jqsrt.2016.04.010.
(59) Larsson, H. R.; Viel, A. 2500 Vibronic Eigenstates of the NO_3 Radical. *Phys. Chem. Chem. Phys.* **2024**. DOI: 10.1039/D4CP02653E.

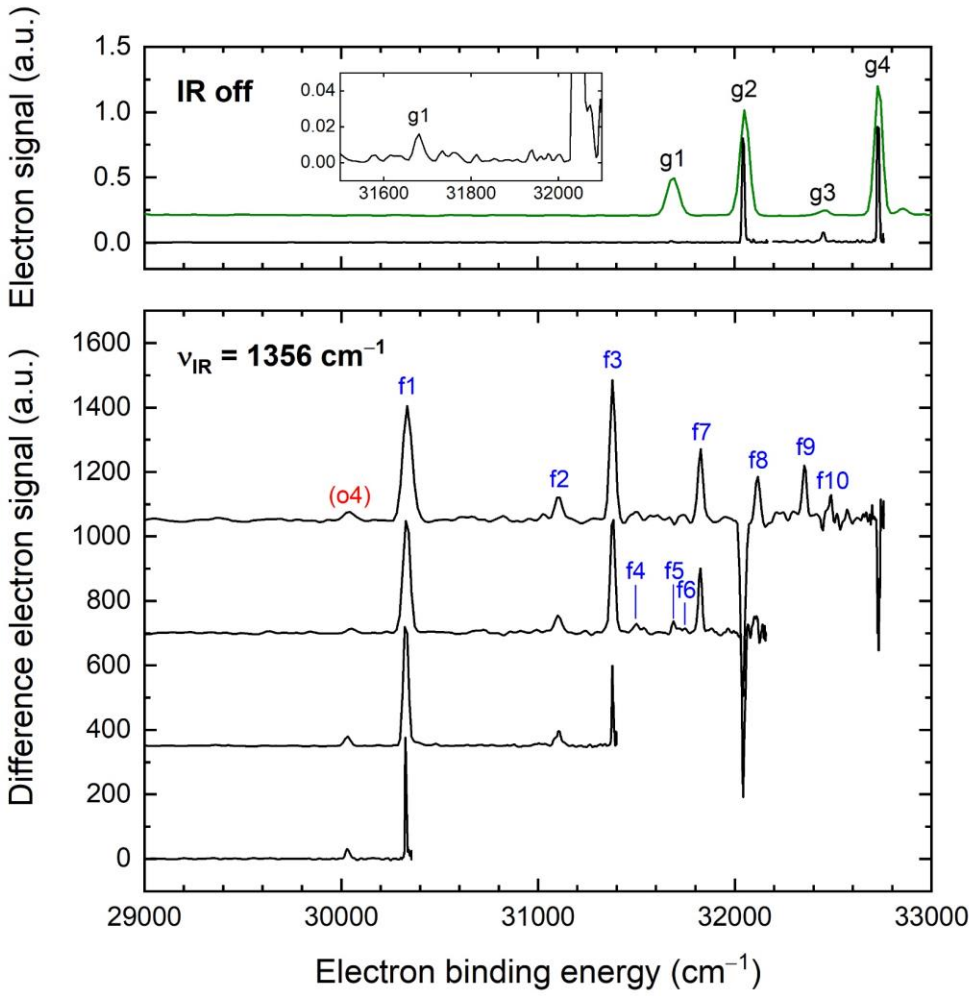

Figure 1. Top panel: Overview (green) and high-resolution (black) photoelectron spectra without IR pre-excitation (IR off). The inset shows the barely detectable vibrational origin peak (g1) for the highest-resolution spectrum. Note that the intensity of g1 in the overview spectrum is substantially higher because of the higher photon energy of 34841 cm^{-1}. Main panel: (IR on)-(IR off) photoelectron spectra of NO_3^- after IR excitation at 1356 cm^{-1}, taken at increasingly lower photodetachment energies and improved resolution (from top to bottom). Peaks labeled f1-f10 are attributed to fundamental ν_3 excitation in the anion. Only the peak labeled o4 is a residual peak from the additional $2\nu_3$ excitation seen in Fig. 2.

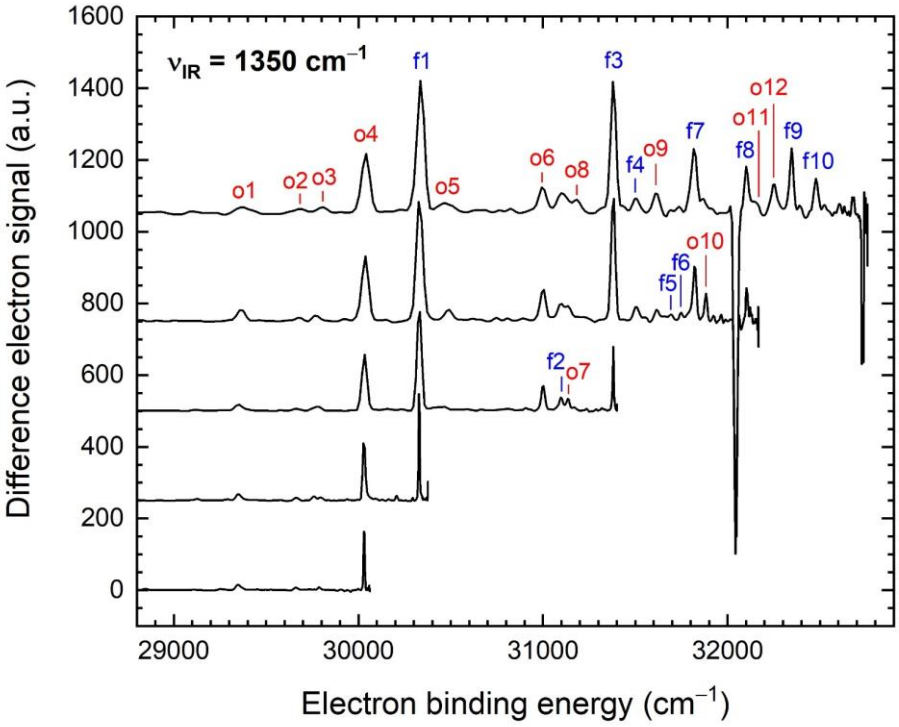

Figure 2. (IR on)-(IR off) photoelectron spectra of NO_3^- after IR after excitation at 1350 cm^{-1}, taken at increasingly lower photodetachment energies and improved resolution (from top to bottom). Peaks labeled f1-f10 indicate the same peaks that are also observed for 1356 cm^{-1} excitation (see Fig. 1). The additional peaks observed only for 1350 cm^{-1} excitation are labeled o1-o12.

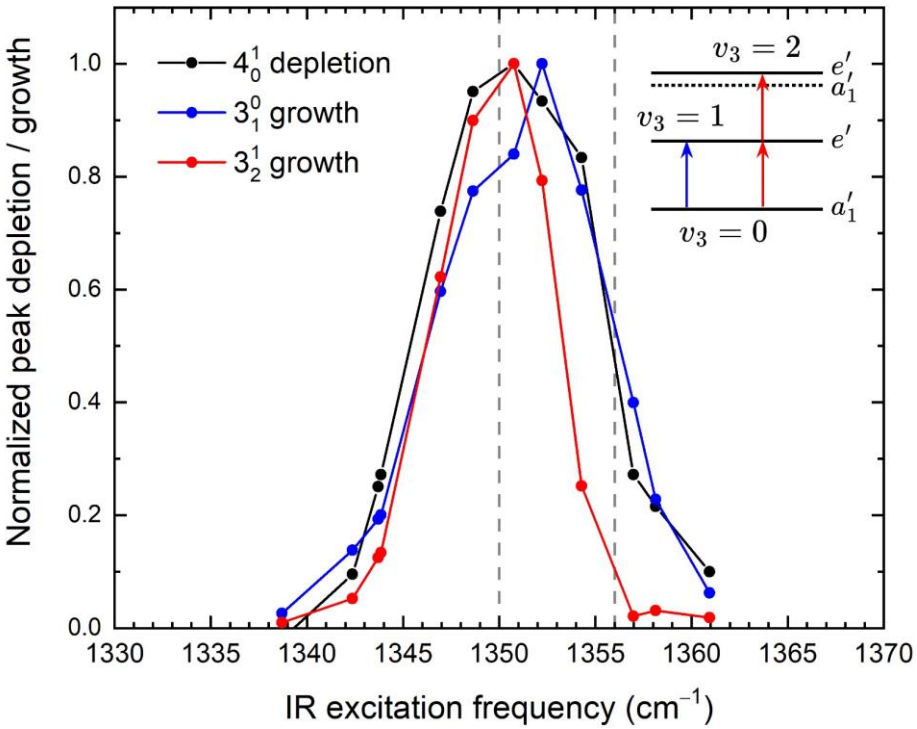

Figure 3. IR action spectrum of NO_3^- taken with a step size of ~2.5 cm^{-1} while monitoring either depletion of the 4_0^1 peak (black dots), growth of the 3_1^0 peak (peak f1, blue dots) or growth of the 3_2^1 peak (peak o4, red dots) in the IR on spectra for each excitation frequency relative to the 4_0^1 peak in the corresponding IR off spectra. Note that all action spectra are additionally normalized to a peak value of 1 for ease of comparison. Gray, dashed lines indicate the excitation frequencies of 1356 and 1350 cm^{-1} used in Figs. 1 and 2, respectively. The energy level diagram in the upper right corner indicates the fundamental and overtone levels accessed via one and two-photon excitation at IR frequencies near 1350 cm^{-1}, corresponding to the blue and red action spectra, respectively.

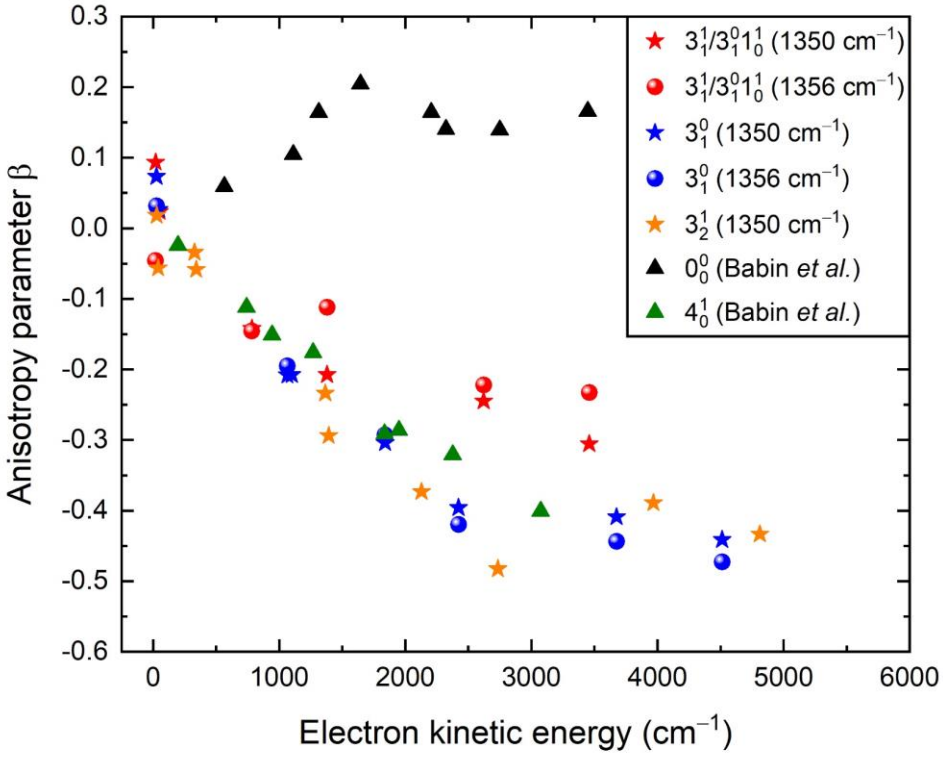

Figure 4. Anisotropy parameters as a function of electron kinetic energy for selected transitions involving the ν_3 mode. Anisotropy parameters for the 3_1^1 and $3_1^0 1_0^1$ (peak f3, red symbols), 3_1^0 (peak f1, blue symbols), and 3_2^1 (peak o4, orange symbols) are extracted from the IR-cryo-SEVI spectra for 1050 and 1056 cm^{-1} IR pre-excitation (represented by stars and dots, respectively). Anisotropy parameters for the ground-state cryo-SEVI transitions 0_0^0 and 4_0^1, shown as black and green triangles, respectively, are taken from Ref. 26.

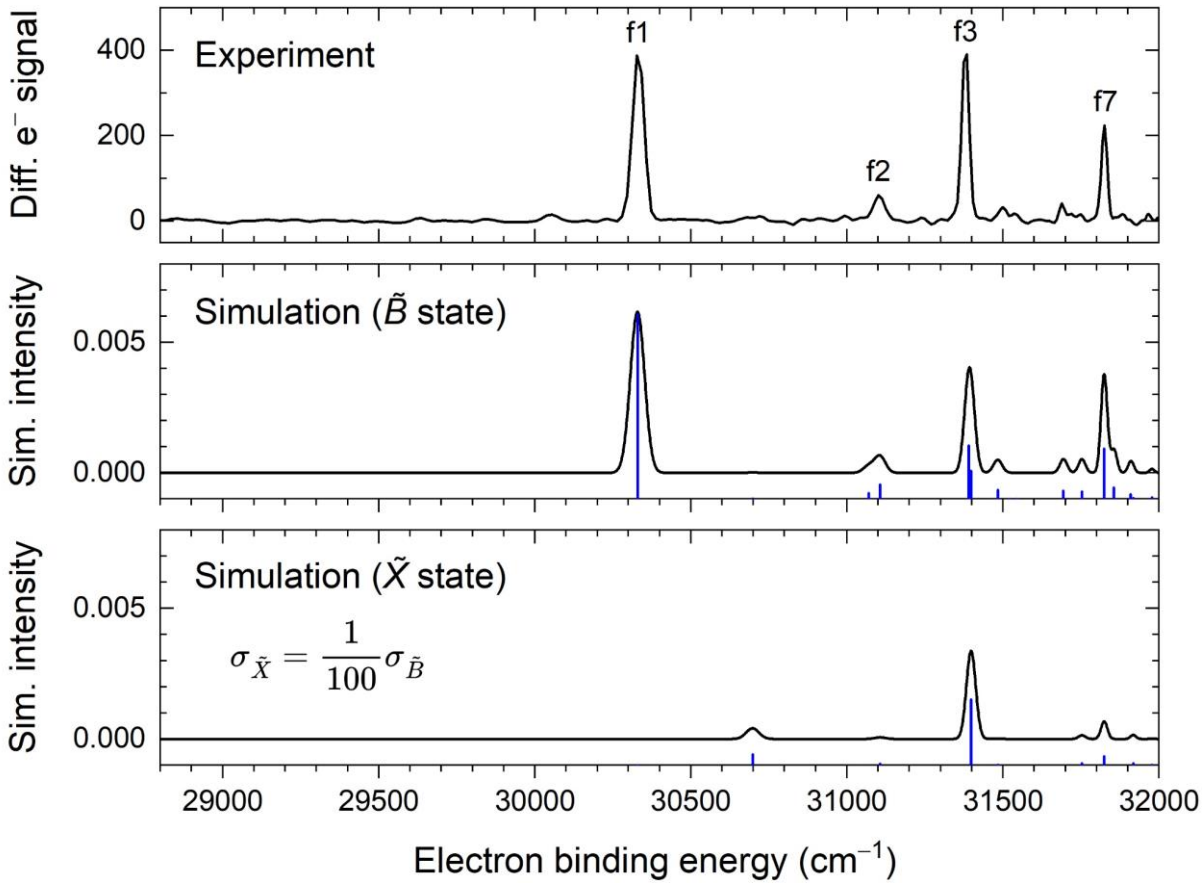

Figure 5. Upper panel: Experimental NO_3^- photoelectron spectrum measured at a detachment energy of 32168 cm^{-1} following IR excitation at 1356 cm^{-1}. Only selected peaks are highlighted by labels. Middle panel: Simulated photoelectron spectrum following excitation of the anion ν_3 level (blue stick spectra) at the same detachment energy as the experiment. Only contributions from the $\tilde{B}$ (diabatic) electronic state are shown by setting the detachment cross section into the $\tilde{X}$ state to 0. The solid black line shows a convolution of the stick spectrum with Gaussians assuming an eKE-dependent linewidth extracted from the experimental spectra. Bottom panel: Equivalent to the middle panel except that here only contributions from the $\tilde{X}$ state are shown by setting the detachment cross section into the $\tilde{B}$ state to 0. The $\tilde{X}/\tilde{B}$ state photodetachment cross section ratio is assumed to be independent of binding energy and equal to 1/100. The simulated intensities, although in arbitrary units, include this intensity ratio and therefore relative intensities between the middle and bottom panels are accurately reflected.

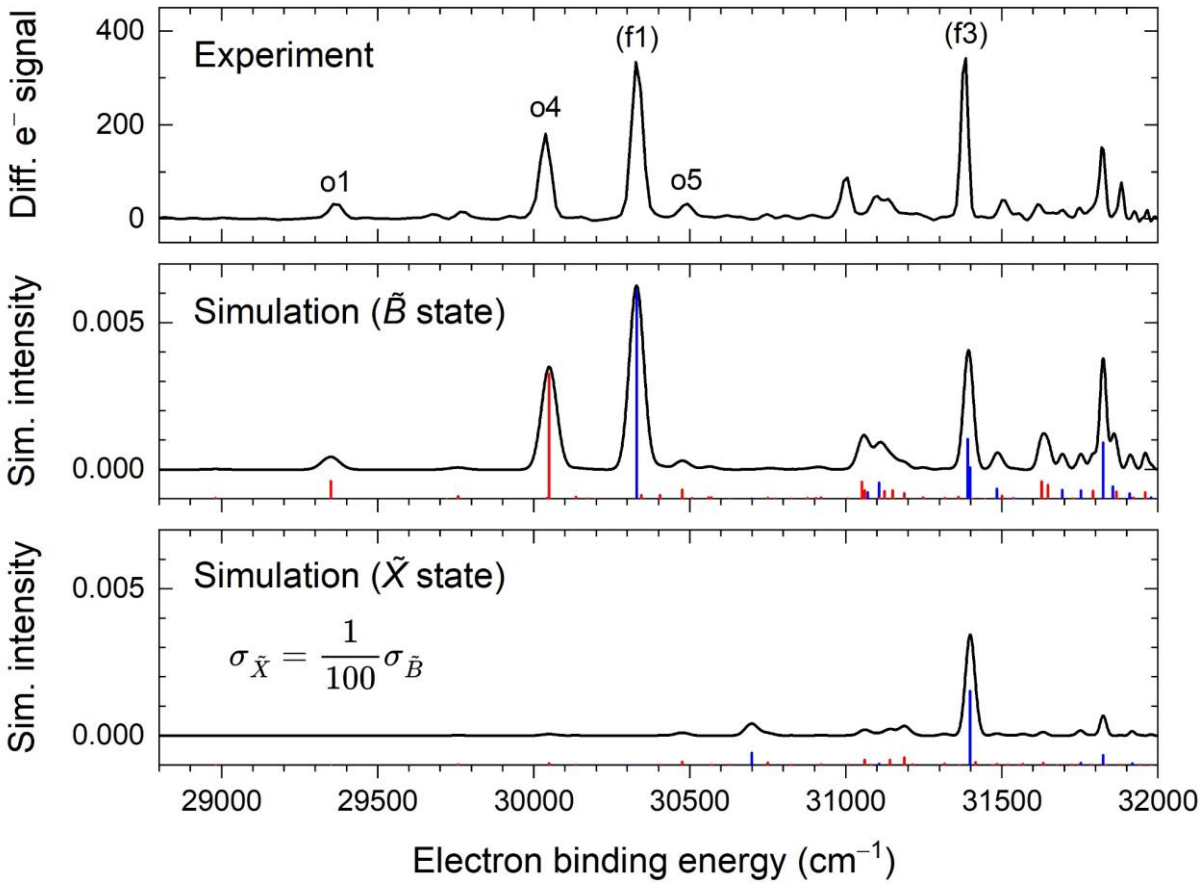

Figure 6. Upper panel: Experimental NO_3^- photoelectron spectrum at a detachment energy of 32168 cm^{-1} following IR excitation at 1350 cm^{-1}. Only selected peaks are highlighted by labels. Middle panel: Simulated spectra resulting from simultaneous excitation of the anion ν_3 level (blue stick spectra) and $2\nu_3(e')$ level (red stick spectra) of the anion at the same detachment energy as the experiment. Only contributions from the $\tilde{B}$ (diabatic) electronic state are shown by setting the detachment cross section into the $\tilde{X}$ state to 0. The relative $2\nu_3$ contribution is chosen such that the combined spectrum reproduces the relative intensities of the o4 and f1 peaks observed experimentally. The solid black line shows a convolution of the red and blue stick spectra with Gaussians assuming an eKE-dependent linewidth extracted from the experimental spectra. Bottom panel: Equivalent to the middle panel except that here only contributions from the $\tilde{X}$ state are shown by setting the detachment cross section into the $\tilde{B}$ state to 0. The $\tilde{X}/\tilde{B}$ state photodetachment cross section ratio is assumed to be independent of binding energy and equal to 1/100. The simulated intensities, although in arbitrary units, include this intensity ratio and therefore relative intensities between the middle and bottom panels are accurately reflected.

Table 1. Selected photodetachment features observed in the cryo-SEVI (IR off) spectra originating from the vibrational ground state of NO_3^-.

Peak	eBE (cm^{-1})[a]	Assignment[b]	Shift from 0_0^0 (cm^{-1})	KDC	Kawaguchi (Ref. 12)
g1	31680(9)	0_0^0	0	0	0
g2	32044(6)	4_0^1	364	369	365.5
g3	32451(8)	$4_0^2\ (e')$	771	777	771.8
g4	32731(6)	3_0^1 and 1_0^1	1051	1069 and 1061	1054.1 and 1051.0

a) Electron binding energies are determined from Gaussian fits to the highest-resolution spectrum for that peak, and the uncertainties in parentheses are estimated as 1σ based on the widths of the Gaussian fits.

b) Symmetry labels in parentheses indicate the vibrational symmetry of the final neutral state.

Table 2. Photodetachment features observed in the IR-cryo-SEVI spectra originating from the ν_3 vibrationally excited state of NO_3^-.

Peak	eBE (cm^{-1})[a]	Assignment[b]	Shift from 3_1^0 (cm^{-1})	KDC	Kawaguchi (Ref. 12)
f1	30329(3)	3_1^0	0	0	0
f2	31097(12)	$3_1^0 4_0^2\ (e')$	768	777	771.8
f3	31380(3)	3_1^1 and $3_1^0 1_0^1$	1051	1069 and 1061	1054.1 and 1051.0
f4	31503(15)	$3_1^0 4_0^3\ (e')$	1174	1152	1173.6
f5	31693(15)	$3_1^1 4_0^1\ (a_2')$	1364	1365	-
f6	31748(7)	$3_1^0 1_0^1 4_0^1$	1419	1424	1413
f7	31822(8)	$3_1^1 4_0^1\ (e')$	1493	1494	1492.4
f8	32104(6)	$3_1^1 4_0^2\ (e')$	1774	1769	1950
f9	32346(11)	$3_1^2(e')$ polyad[c]	2017	> 2000	2024.3
f10	32479(12)	$3_1^2(e')$ polyad[c]	2149	> 2000	2155

a) Electron binding energies are determined from Gaussian fits to the highest-resolution spectrum for that peak, and the uncertainties in parentheses are estimated as 1σ based on the widths of the Gaussian fits.

b) Symmetry labels in parentheses indicate the vibrational symmetry of the final neutral state.

c) See Section 4.3.3 for a discussion of the levels assigned to transitions into the $2\nu_3(e')$ polyad.

Table 3. Photodetachment features observed in the IR-cryo-SEVI spectra originating from the $2\nu_3(e')$ vibrationally excited state of NO_3^-.

Peak	eBE (cm^{-1})[a]	Assignment[b]	Shift from 3_2^0 (cm^{-1})[c]	Shift from 3_3^0(cm^{-1})[c]	KDC	Kawaguchi (Ref. 12)
o1	29351(15)	$3_2^0 4_0^1$	372	-	369	365.5
o2	29660(10)	3_3^2 (e') polyad[d]	(680)	2030	> 2000	2024.3
o3	29789(9)	3_3^2 (e') polyad[d]	(810)	2160	> 2000	2155
o4	30031(3)	3_2^1	1051	-	1069	1054.1
o5	30488(21)	$3_2^1 4_0^1$ (e')	1508	-	1494	1492.4
o6	31000(10)	3_2^2 (e') polyad[d]	2020	-	> 2000	2024.3
o7	31135(9)	3_2^2 (e') polyad[d]	2155	-	> 2000	2155
o8	31184(23)	3_2^2 (e') polyad[d]	2204	-	> 2000	2205.7
o9	31617(13)	unassigned	2637	-	-	-
o10	31882(7)	$3_1^1 1_0^1 4_0^2$ (e')	2902	-	-	2902
o11	32146(20)	unassigned	3166	-	-	-
o12	32252(17)	unassigned	3272	-	-	-

a) Electron binding energies are determined from Gaussian fits to the highest-resolution spectrum for that peak, and the uncertainties in parentheses are estimated as 1σ based on the widths of the Gaussian fits.

b) Symmetry labels in parentheses indicate the vibrational symmetry of the final neutral state.

c) The positions of the 3_2^0 and 3_3^0 transitions are defined as $EA - 2\tilde{\nu}_{\mathrm{IR}} = 31680\ \mathrm{cm}^{-1} - 2 \times 1350\ \mathrm{cm}^{-1}$ and $EA - 3\tilde{\nu}_{\mathrm{IR}} = 31680\ \mathrm{cm}^{-1} - 3 \times 1350\ \mathrm{cm}^{-1}$, respectively.

d) See Section 4.3.3 for a discussion of the levels assigned to transitions into the $2\nu_3(e')$ polyad.